Author(s): Rontu, Ville; Sippola, Perttu; Broas, Mikael; Ross, Glenn; Sajavaara, Timo; Lipsanen, Harri; Paulasto-Kröckel, Mervi; Franssila, Sami

Title: Atomic layer deposition of AlN from AlCl3 using NH3 and Ar/NH3 plasma

Year: 2018

Version:

Please cite the original version:

Rontu, V., Sippola, P., Broas, M., Ross, G., Sajavaara, T., Lipsanen, H., Paulasto-Kröckel, M., & Franssila, S. (2018). Atomic layer deposition of AlN from AlCl3 using NH3 and Ar/NH3 plasma. Journal of Vacuum Science and Technology A, 36(2), Article 021508. https://doi.org/10.1116/1.5003381

Atomic layer deposition of AlN from $AlCl_3$ using NH_3 and Ar/NH_3 plasma

Ville Rontu, Perttu Sippola, Mikael Broas, Glenn Ross, Timo Sajavaara, Harri Lipsanen, Mervi Paulasto-Kröckel, and Sami Franssila

Citation: Journal of Vacuum Science & Technology A: Vacuum, Surfaces, and Films **36**, 021508 (2018);
View online: https://doi.org/10.1116/1.5003381
View Table of Contents: http://avs.scitation.org/toc/jva/36/2
Published by the American Vacuum Society

Atomic layer deposition of AlN from $AlCl_3$ using NH_3 and Ar/NH_3 plasma

Ville Rontu[a)]
Department of Chemistry and Materials Science, Aalto University, P.O. Box 13500, FIN-00076 Aalto, Espoo, Finland

Perttu Sippola
Department of Electronics and Nanoengineering, Aalto University, P.O. Box 13500, FIN-00076 Aalto, Espoo, Finland

Mikael Broas and Glenn Ross
Department of Electrical Engineering and Automation, Aalto University, P.O. Box 13500, FIN-00076 Aalto, Espoo, Finland

Timo Sajavaara
Department of Physics, University of Jyvaskyla, P.O. Box 35, FIN-40014 Jyvaskyla, Finland

Harri Lipsanen
Department of Electronics and Nanoengineering, Aalto University, P.O. Box 13500, FIN-00076 Aalto, Espoo, Finland

Mervi Paulasto-Kröckel
Department of Electrical Engineering and Automation, Aalto University, P.O. Box 13500, FIN-00076 Aalto, Espoo, Finland

Sami Franssila
Department of Chemistry and Materials Science, Aalto University, P.O. Box 13500, FIN-00076 Aalto, Espoo, Finland

(Received 5 September 2017; accepted 29 December 2017; published 18 January 2018)

The atomic layer deposition (ALD) of AlN from $AlCl_3$ was investigated using a thermal process with NH_3 and a plasma-enhanced (PE)ALD process with Ar/NH_3 plasma. The growth was limited in the thermal process by the low reactivity of NH_3, and impractically long pulses were required to reach saturation. Despite the plasma activation, the growth per cycle in the PEALD process was lower than that in the thermal process (0.4 Å vs 0.7 Å). However, the plasma process resulted in a lower concentration of impurities in the films compared to the thermal process. Both the thermal and plasma processes yielded crystalline films; however, the degree of crystallinity was higher in the plasma process. The films had a preferential orientation of the hexagonal AlN [002] direction normal to the silicon (100) wafer surface. With the plasma process, film stress control was possible and tensile, compressive, or zero stress films were obtained by simply adjusting the plasma time. *Published by the AVS.* https://doi.org/10.1116/1.5003381

I. INTRODUCTION

AlN films are used in a variety of applications, such as sensors,[1] actuators,[2] high-power integrated circuits (ICs),[3,4] and light-emitting diodes,[5,6] which take advantage of the excellent thermal, piezoelectric, dielectric, or wide bandgap semiconductor properties of AlN. These films have typically been deposited using metal-organic chemical vapor deposition (MOCVD) for IC applications[3,4] or by sputtering for microelectromechanical system (MEMS) applications.[7,8] MOCVD films have yielded films with the highest quality, but the deposition process requires high temperatures close to 1000 °C. This limits the available substrates and induces large stresses in the films due to mismatch in the coefficients of thermal expansion between the substrate and the film. Sputtering on the other hand is inadequate in terms of film uniformity and conformality for some MEMS applications.

Atomic layer deposition (ALD) of AlN has been investigated in the past mainly using trimethylaluminum ($AlMe_3$) as the Al precursor.[9–19] The as-deposited films have had varying degrees of crystallinity ranging from amorphous films[11,18] to polycrystalline films with no preferential orientation[9,12,13,16] to epitaxial films.[14,19] Due to the use of $AlMe_3$ as the aluminum precursor, these films have often had a high concentration of hydrogen[9,11,15,18] and carbon impurities.[9–11,14–18]

NH_3 has been almost exclusively used as the coreactant in the thermal ALD of nitrides.[20] However, NH_3 typically requires high temperatures to be reactive. For instance, below 450 °C in an $AlMe_3$ based AlN process, the low reactivity of NH_3 has been observed to result in incomplete elimination of CH_3 ligands[21] and can lead to incorporation of C and H into the film. However, $AlMe_3$ starts to decompose above 325 °C,[21] which also can cause some C contamination in the growing films at temperatures above this. Due to these reasons, plasma-enhancement has been widely used with the aim of depositing AlN films of higher quality.[11–19]

The highly reactive plasma radicals in plasma-enhanced ALD (PEALD) allow the deposition of films with higher density and lower impurity concentration compared to a

[a)]Electronic mail: ville.rontu@aalto.fi

thermal process of the same temperature.[22] Plasma-enhancement has indeed led to the decrease of C impurities in AlN films deposited from $AlMe_3$ compared to the equivalent thermal AlN process.[17] However, a few percent of C has been found in the films.[14,16,17] In addition, incorporation of up to 20 at. % H has been observed in PEALD films.[11,15,18] The H in the films is often ignored, as only a few measurement systems are able to detect it. The increasing H concentration decreases the film density and refractive index[11] and may cause blistering during annealing as has been observed in the case of Al_2O_3.[23]

Only a few publications exist on the deposition of AlN from $AlCl_3$. The thermal deposition of AlN from NH_3 was investigated by Elers *et al.*[24] and Jokinen *et al.*[25] two decades ago and more recently by Lee *et al.*[26,27] using $Ar/H_2/NH_3$ plasma. The results showed a large concentration of Cl impurities in the thermal ALD AlN films from $AlCl_3$, whereas the PEALD AlN films had a very low impurity concentration with a preferential orientation of the AlN [002] axis normal to the silicon substrate (100) surface. Despite these promising results, the PEALD AlN process from $AlCl_3$ has not sparked more studies on the topic.

Deposition of oriented AlN films with a low concentration of impurities could open up applications for PEALD AlN in nanoelectromechanical systems (NEMSs). For instance, RF NEMS requires thin piezoelectric membranes with low stress. Possibility to affect the residual stress state has been demonstrated for PEALD films by applying bias voltage between the substrate and plasma.[28] Yet, this possibility has been sparsely studied.

This research covers growth, density, refractive index, crystallinity, and elemental composition studies of thermal and plasma-enhanced ALD of AlN from $AlCl_3$ and NH_3. Moreover, characterization methods are used to show the effect of plasma time on the growth, impurities, structural quality, and residual stress of the AlN films.

II. EXPERIMENT

A. Film deposition

The AlN films were deposited in a Picosun R200 plasma ALD tool which utilizes remote inductively coupled plasma. A plasma power of 2000 W was used in the plasma-enhanced process. The reactor pressure during deposition was a few hectopascals. $AlCl_3$ (>99.99%, Sigma-Aldrich) delivery from a heated source to the reactor was boosted with N_2 (99.9999%, Aga) by closing the pulsing valve at high line flow and opening at low line flow. NH_3 (99.999%, Aga) was used for both thermal and plasma processes. Ar (99.9999%) was constantly flowing through the plasma generator and N_2 through other precursor delivery lines. The thermal process was carried out at a reactor set temperature of 500 °C, which corresponded to approximately a 475 °C wafer temperature when a stainless steel lid was inserted between the plasma unit and the reactor. The temperature difference between the reactor set temperature and the actual wafer temperature was due to a heat balance in the vacuum chamber between a hot bottom and a colder plasma generator. The lid blocked the direct gas flow from the plasma unit to the substrate, allowing higher wafer temperatures than without the lid. The lid also acted as a showerhead, enhancing the precursor spreading. The plasma process was carried out without the lid at a reactor set temperature of 500 °C corresponding to a wafer temperature of approximately 425 °C. Later in this manuscript, the wafer temperatures are used to communicate the process temperature. 150 mm, (100) Si wafers were used as the substrates. The wafers were cleaned prior to deposition using the RCA cleaning process consisting of SC-1, HF, and SC-2, resulting in an amorphous chemical oxide on the wafer.

B. Characterization

The wafer curvature before and after deposition was measured using a FLX 2320S measurement system, which uses the deflection of a laser beam to determine the curvature. Stoney's equation was used to calculate the film stress, and the measurement error was calculated using total differential as described by Ylivaara *et al.*[29]

The film thickness and refractive index were measured using a Plasmos SD2300 single wavelength ellipsometer utilizing a HeNe laser at a wavelength of 632.8 nm and at the incident angle of 70°. On a 150 mm wafer, 9–13 points were measured and the values were extracted using a one-layer model for the final iterative data fitting.

X-ray reflectivity (XRR) analyses were performed with a Philips X'Pert Pro diffractometer using the Cu $K_{\alpha 1}$ radiation. The densities and thicknesses were acquired from the measured data by using an in-house developed fitting software.[30] In order to obtain the best fit, an interfacial oxide layer between the silicon substrate and the AlN film was simulated as a part of the XRR fitting layer model.

Symmetrical θ-2θ x-ray diffraction (XRD) and wide area diffraction maps (χ-2θ space) were measured using an x-ray diffractometer (Rigaku SmartLab) equipped with a 9 kW rotating Cu anode source. In the θ-2θ scans, the incident beam was monochromatized using a multilayer mirror and a Ge(220) double-bounce monochromator. The wide area diffraction maps were obtained without a monochromator using a 2D-detector.

Electron-transparent lamellas were prepared with focused ion beam systems (FEI and Zeiss) using either *in situ* or *ex situ* liftout. Pt, C, or both were used as the protective layers. Transmission electron microscopy (TEM) was conducted with three systems: (1) at 300 kV with an image Cs-corrected FEI Titan^3 G2 60–300, (2) at 200 kV with a JEOL JEM-2800, or (3) at 200 kV with a FEI Tecnai F20-FEGTEM S-Twin. Care was taken on not to irradiate the samples for a prolonged time with the electron beam to avoid accidental crystallization.

Time-of-flight elastic recoil detection analysis (ToF-ERDA) was performed using equipment described in Ref. 31. The samples were measured using an 11.915 MeV $^{63}Cu^{7+}$ ion beam, and the data were analyzed using a POTKU analysis software.[32]

III. RESULTS AND DISCUSSION

A. Film growth characteristics

Precursor dosing was investigated in the thermal process at 475 °C by depositing 1000 cycles on the (100) Si wafer. At first, the $AlCl_3$ dose was varied by changing the $AlCl_3$ source bottle temperature with a fixed 4 s NH_3 pulse time [Fig. 1(a)] and second using an optimal $AlCl_3$ dose and varying the NH_3 pulse time [Fig. 1(b)]. The $AlCl_3$ dose reached a saturation at a source bottle temperature between 160 and 165 °C. The source bottle temperature of 162 °C was used for the subsequent depositions with the NH_3 pulse time as a variable. Long NH_3 pulses were required to reach a saturation, indicating a poor reactivity with the surface. For comparison, 0.1 s NH_3 pulsing is enough to reach the saturation in a thermal TiN process with $TiCl_4$ using the same reactor setup. The growth-per-cycle (GPC) of the thermal AlN process at 475 °C was 0.7–0.8 Å. At 450 °C, the GPC decreased to 0.6 Å.

At least 1000 cycles of PEALD AlN were deposited at 425 °C using the same $AlCl_3$ parameters, i.e., bottle temperature and pulsing, as was used in the thermal process. Ar/NH_3 plasma at a power of 2000 W was used as the coreactant in an AB process. The flow rate of Ar was 40 sccm and controlled by a mass flow controller, while the flow rate of NH_3 was approximately 40 sccm controlled by a needle valve. Higher NH_3 flow rates were outside of the optimal operation condition for the plasma generator and could not be used. In order to increase the amount of reactive species during the plasma pulse, an ABC type scheme was designed, where between the $AlCl_3$ and the plasma pulses, NH_3 was pulsed for 0.5 s into the reactor without RF power. NH_3 was pulsed through a different pulsing valve allowing a higher NH_3 flow than during the plasma pulse. After this NH_3 pulse, no purging was done. This was done to plasma activate some of the NH_3 still present inside the reactor and thus increase the number of reactive species without increasing the plasma time. As a consequence, the GPC increased slightly (Fig. 2). Average GPC at the plasma time of 3 s was 0.29 Å for the AB process and 0.33 Å for the ABC process. However, there was variation from run to run. A possible reason for the variation was inconsistent precursor dosing. For instance, the NH_3 flow through the plasma generator drifted ±10 sccm according to the mass flow meter. The benefit of the ABC type process was more pronounced on the refractive index, which was 1.84 for the AB process and 1.92 for the ABC process with the plasma time of 3 s. Film blistering was observed occasionally on samples with a plasma time of over 6 s. On these samples, the whole wafer might have been full of blisters or then the blisters were more localized.

B. Film properties

The effect of plasma time on the residual stress of the deposited AlN films was studied. It was found that with the increasing plasma time, the film stress shifted toward more compressive. Figure 3(a) presents the film stress as a function of plasma time. A short plasma time of 2 s led to a film with tensile stress, at 3 s, the stress was close to zero, and at 4 s and longer plasma times, the films displayed high compressive stresses.

Together with the shift of the residual stress toward more compressive with the longer plasma times, the film density [Fig. 3(b)] and the refractive index increased [Fig. 3(c)]. Using the plasma time of 3 s, the ABC process resulted in films with a higher refractive index (1.92) and density (2.84 g/cm^3) than the corresponding 3 s AB process (1.84 and 2.72 g/cm^3). In addition, the XRR analysis revealed that the AlN film with the 3 s AB process had a subnanometer thick surface layer with lower density, thus indicating minor post-PEALD oxidation of the AlN surface. For the ABC process, an oxidized surface layer was not observed with XRR,

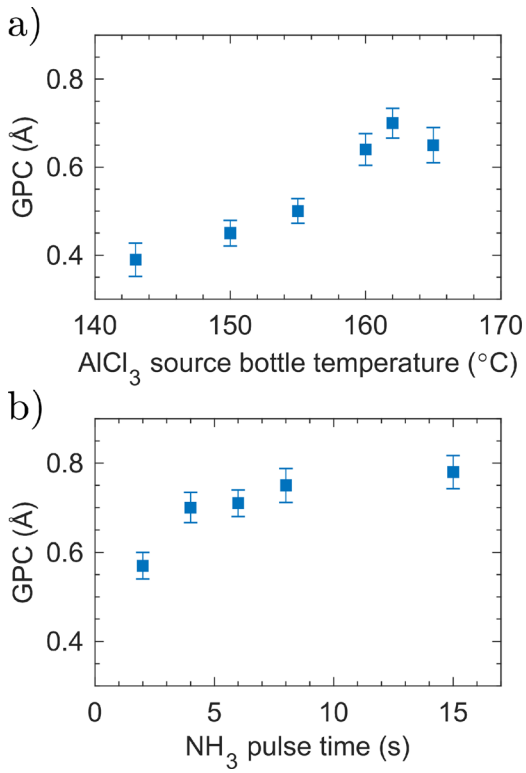

FIG. 1. (Color online) GPC as a function of (a) $AlCl_3$ source bottle temperature and (b) NH_3 pulse time.

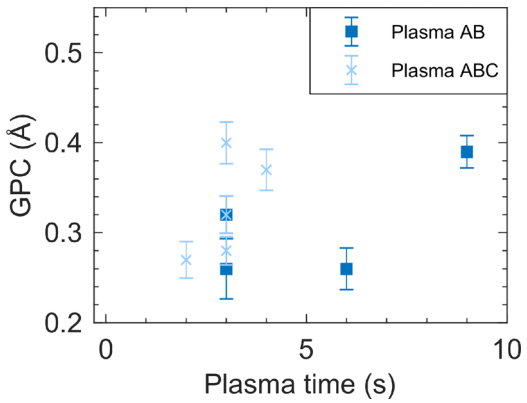

FIG. 2. (Color online) GPC as a function of plasma time for the AB and ABC processes.

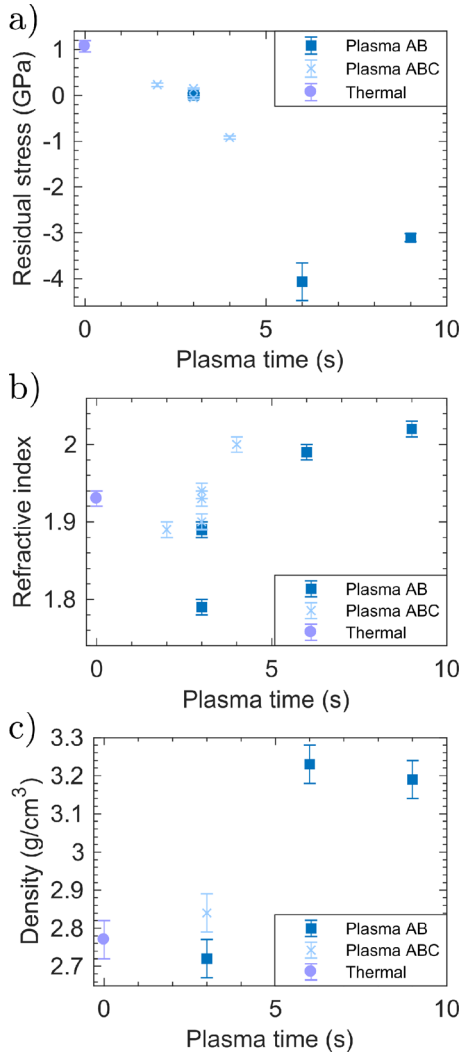

FIG. 3. (Color online) (a) Residual stress, (b) refractive index, and (c) density as a function of plasma time. The deposition temperatures were 425 °C during the plasma processes and 475 °C during the thermal process. The films were deposited with 1000–2200 cycles resulting in 27–77 nm thick films.

showing improved stability in comparison to the AB process. The ABC process with a plasma time of 3 s yielded films with similar properties in terms of refractive index and density as the thermal process that was deposited at a higher temperature.

The AlN films were crystalline according to the θ-2θ XRD scans (Fig. 4). Both thermal and PEALD films (AB 6 s and ABC 3 s) show a single distinct peak corresponding to the hexagonal (002) plane. The full width at half maximum (FWHM) peak center positions were 35.92° for the thermal, 35.96° for the plasma ABC, and 35.48° for the plasma AB films. The (002) peaks have shifted according to a biaxial compressive stress in all cases compared to the database peak locations[33] [36.04° for the (002) peak] obtained from the Inorganic Crystal Structure Database.[34] However, the thermal film is in a biaxial tensile stress based on the wafer curvature data. The plasma AB film is in high compressive stress also according to the XRD measurement, while the plasma ABC film shows a small shift compared to the database peak location. The films are not ideal bulk AlN because

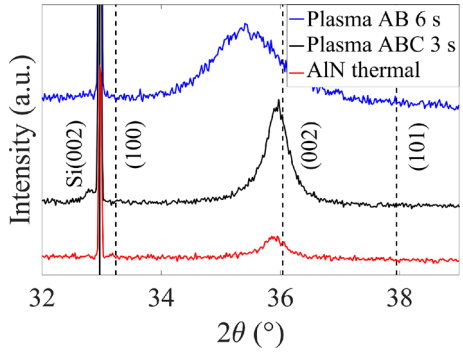

FIG. 4. (Color online) θ-2θ scan for thermal and PEALD AlN films. They are presented in the same order as in the legend. All films show only a single peak belonging to the (002) plane of hexagonal AlN. The film thicknesses were 71 nm for thermal, 56 nm for plasma ABC 3 s, and 58 nm for plasma AB 6 s.

of impurities coming from the deposition process. The impurities may affect the ideal AlN lattice constants, highlighting the fact that relying on only θ-2θ XRD measurements can be insufficient when measuring the film stress using bulk material lattice constants as references. Nevertheless, the peak positions give an indication of the magnitude of the biaxial stress (low for the thermal and ABC process and very high for the AB process). Furthermore, the AB plasma process film shows a considerably broadened peak, indicating that the grains are small and have a high defect density likely related to the high compressive stress.

The wide area diffraction 2D maps (Fig. 5) show the tilt of the AlN grains in addition to the peak positions and their broadening, which was also seen in the θ-2θ 1D scans [Fig. 4]. The χ angle can be used to approximate the FWHM values of the plasma process films, being more than 20° for both. That is, the tilt of the grains with respect to the normal of the substrate comprises a sector of more than ±10°. The (002) peak of the thermal process film has a very low intensity compared to the plasma-based films, indicating a lower degree of crystallinity.

TEM was conducted on the films to further investigate their crystallinity. Figures 6–8 show bright-field TEM (BFTEM), high-resolution TEM (HRTEM), and selected area electron diffraction (SAED) images. Note that three different TEMs and cameras were used in obtaining the images, making them visually slightly different. The SAED aperture was used to select both the Si substrate and the film in all SAED images. All TEM images were taken along the Si ⟨110⟩ zone axis, and the bright, unindexed reflections belong to Si.

The films show polycrystalline structures. A slight preferred orientation is observed in the plasma-based films with the hexagonal c-axis normal to the surface (see the 002 reflections in the SAED images of Figs. 6–8). Furthermore, based on the BFTEM and HRTEM images in Figs. 7 and 8, it is found that the grains seem to grow in a columnar fashion, therefore giving rise to a higher intensity in the 002 reflections [or (002) XRD peaks]. The grains in the thermal film seem to be smaller in size [Fig. 6(b) versus Figs. 7(b) and 8(b)] and more randomly distributed within the film.

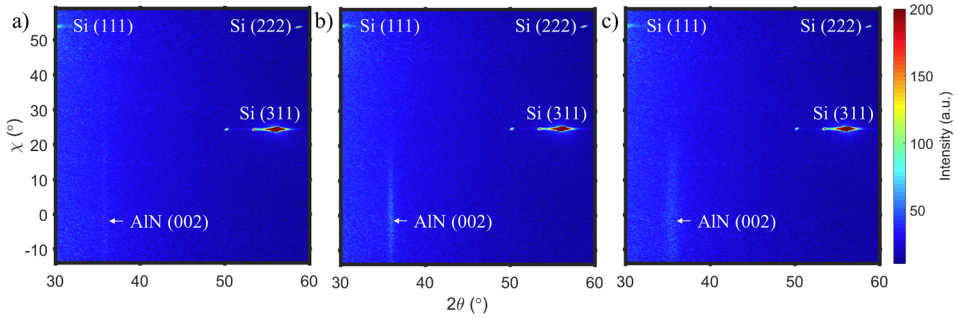

FIG. 5. (Color online) Wide area diffraction maps of (a) thermal, (b) plasma ABC 3 s, and (c) plasma AB 6 s AlN films. The χ angle is the rotation of the sample parallel to the beamline, giving the rotation of the AlN hexagonal c-axis with respect to the substrate normal.

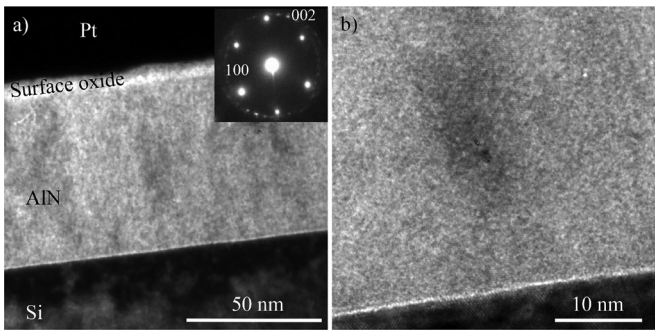

FIG. 6. TEM images of the thermal AlN film. An overview image (a) with a small objective lens aperture (high diffraction contrast) shows a partly crystalline structure, while the HRTEM image (b) at the Si-AlN interface shows lattice planes corresponding to small crystallites. The protective Pt layer has been deposited using evaporation (dense Pt).

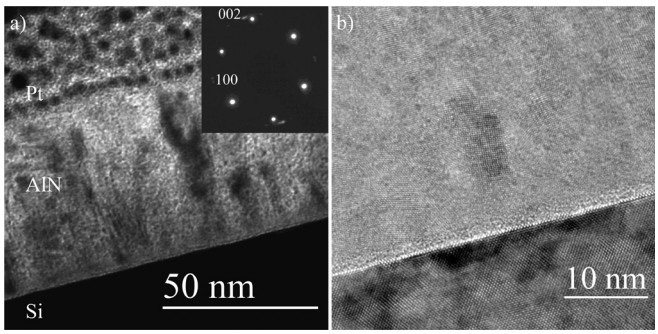

FIG. 7. TEM images of the plasma ABC 3 s process film. (a) BFTEM and SAED image. (b) HRTEM at the Si-AlN interface. The protective Pt layer has been deposited using a FIB (less dense Pt).

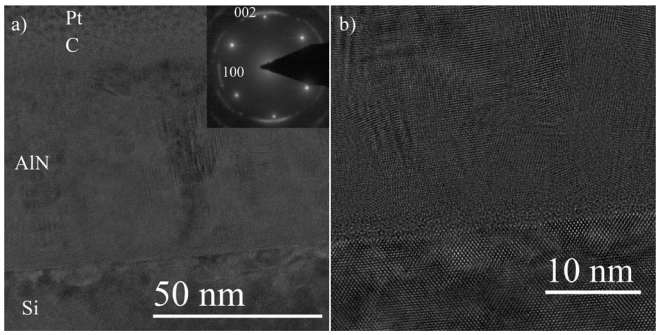

FIG. 8. TEM images of the plasma AB 6 s process film. (a) BFTEM and SAED image. (b) HRTEM at the Si-AlN interface. Evaporated carbon and FIB-assisted Pt were used as the protective layer.

The thermal sample also has an area of bright contrast in Fig. 6(a), scattering the electron beam less, most likely coming from a distinct surface oxide. Finally, the plasma-enhanced samples have a distinct amorphous layer (2–3 nm) between the crystalline AlN and the Si substrate. Part of the amorphous layer is chemical SiO_2 from the SC-2 cleaning, but it is too thick to be simply the oxide layer. The thermal film does not display such a distinct layer although differentiating between the bulk film and an interfacial layer is challenging due to the low degree of crystallinity of the sample and the resolution of the image.

Elemental compositions (Table I) were determined by ToF-ERDA. The films are slightly N rich with H, O, and Cl as the main impurities. Notable is that in addition to the highest Cl concentration (3.8 at. %), the highest H concentration (10.9 at. %) was also observed from the thermal AlN film, which is indicative of incomplete surface reactions during both precursor pulses. In the thermal process, the Cl and H incorporation is a result of incomplete elimination of -$AlCl_x$ and -NH_x surface species, respectively. The lowest impurity concentration (6.5 at. % H, 0.1 at. % Cl) was observed in the plasma AB 6 s AlN film, demonstrating that the long plasma pulse is required to remove Cl ligands from the surface. The fairly high H concentration in the PEALD films can be a result of both incomplete elimination of -NH_x surface species and H incorporation into the film during the plasma pulse. The long plasma pulses, however, also led to large compressive residual stresses as observed by XRD and wafer curvature measurements. This is likely due to an Ar bombardment of the growing film since 0.06 at. % of Ar was measured in the plasma AB 6 s film even though the tool utilizes a remote (downstream) plasma and no substrate biasing. The Ar concentration was below the detection limit (<0.05 at. %) in the plasma ABC 3 s AlN film, which can be credited to the shorter plasma time. The origin of the oxygen in the films is likely from residual oxygen and small leaks in the vacuum chamber, despite the fact that the chamber was conditioned prior to AlN deposition by depositing TiN until its resistivity saturated. The saturation of TiN resistivity is an indication that the residual oxygen has been removed from the chamber as the oxygen impurity concentration increases TiN resistivity. However, the thermal, plasma AB, and ABC series were deposited at different times, and the tool condition may not have been identical between the runs.

TABLE I. Elemental compositions of the AlN films as determined by ToF-ERDA. Values are integrated from the film bulk, excluding the surfaces and interfaces. All units are in at. %.

	Al	N	H	O	Cl	C	Ar	F
Thermal	41 ± 2	44 ± 2	10.9 ± 0.8	0.9 ± 0.2	3.8 ± 0.4	0.06 ± 0.03	<0.05	0.21 ± 0.05
Plasma ABC 3 s	43 ± 2	44 ± 2	8.2 ± 0.8	3.1 ± 0.3	1.9 ± 0.2	0.09 ± 0.04	<0.05	—
Plasma AB 6 s	45 ± 2	47 ± 2	6.5 ± 0.6	1.7 ± 0.07	0.1 ± 0.2	0.09 ± 0.02	0.06 ± 0.01	—

In addition to elements discussed above, a small concentration of C (< 0.1 at. %) was observed in all the films, while in addition, F (0.21 at. %) was measured in the thermal AlN film. The origin of F in the thermal AlN film is unknown.

Figure 9 shows ToF-ERDA depth profiles where surface oxidation is clearly visible. The surface of the thermal AlN is completely oxidized, whereas the PEALD films show less oxidation (Fig. 9). The H and C concentrations also peak at the surface.

C. Discussion

The results of the thermal ALD AlN process show that the NH_3 reactivity at 475 °C is not high enough to completely remove Cl ligands from the surface even with long NH_3 pulses. However, the measured Cl concentration (3.8 at. %) was lower compared to an earlier study (6 at. %) where the deposition temperature was 500 °C.[25] Higher temperatures should be used for thermal deposition of AlN from $AlCl_3$ and NH_3 in order to deposit Cl-free films. However, such temperatures are beyond most current ALD systems. In addition, higher temperatures will result in higher residual stresses due to the mismatch of coefficients of thermal expansion between the film and the substrate.

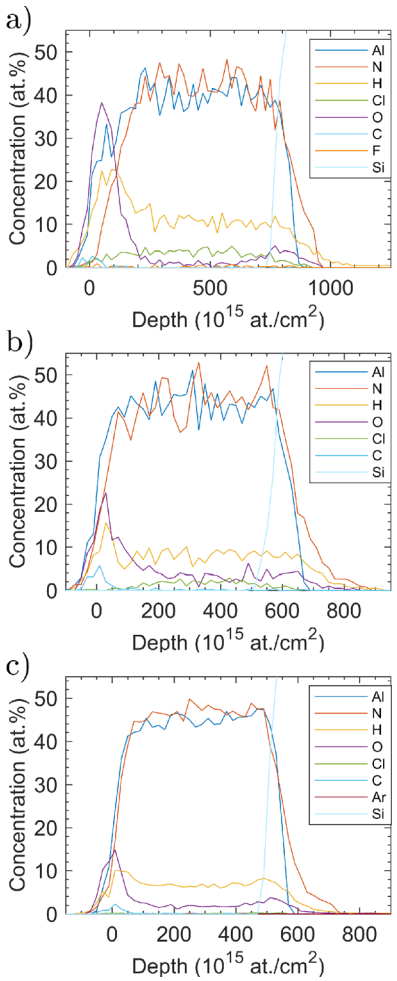

FIG. 9. (Color online) ToF-ERDA depth profile for (a) thermal, (b) plasma ABC 3 s, and (c) plasma AB 6 s AlN films. The film thicknesses were 71 nm for thermal, 56 nm for plasma ABC 3 s, and 58 nm for plasma AB 6 s.

The GPC of the PEALD process was lower than that of the thermal process (0.4 Å vs 0.7 Å) despite the fact that an increase of the GPC is often observed for PEALD processes.[22] The differences of the GPCs between thermal and plasma processes have been related to a higher density of reactive sites on the surface due to the high reactivity of plasma.[22] In the thermal process, the incomplete removal of Cl ligands leads to the incorporation of Cl and may prevent the rearrangement of atoms on the surface, impairing crystallization and producing a less dense structure which results in an increase of the GPC. The remaining Cl ligands also block growth in the subsequent pulse. When the surface coverage becomes large enough, the remaining Cl ligands start to limit the GPC, explaining the lower GPC of the 450 °C thermal process compared to the thermal process at 475 °C. In contrast to the thermal process, in the plasma process, not only the Cl ligands are effectively removed from the surface but also the ion bombardment further contributes to the densification of the film. The $AlCl_3$ pulse may also affect the GPC as the dosing was optimized at 475 °C and was not changed for depositions at lower temperatures. However, Lee and Kang[26] also observed low GPC of 0.42 Å for their PEALD AlN process at 350 °C.

The plasma time was observed to affect the residual stress, refractive index, and film density. The refractive index and film density increased, while the residual stress became more compressive. Because these properties appear to be coupled, residual stress should be measured when optimizing film properties as it can affect the applications. A small tensile stress can be advantageous for membrane applications to keep the membrane flat. A high compressive stress might impose problems such as blistering,[23] which was observed for some samples with longer plasma times.

The deposited films were polycrystalline and showed the preferred hexagonal AlN [002] direction normal to the silicon (100) surface orientation in the XRD and SAED patterns. However, the χ-2θ scans showed a large FWHM range (>20°). For sputtered AlN films, (002) rocking curve FWHM values <10° have been demonstrated even for films thinner than 100 nm.[1,2] The FWHM values are, however,

largely substrate and thickness dependent.[2,35] In order to improve the crystallinity, the deposition process should be further optimized and the effect of suitable seed layers needs to be investigated.

The AlN films deposited from $AlCl_3$ had fewer impurities than what is commonly observed for AlN films deposited from $AlMe_3$.[11,15,18] For instance, H concentrations in our PEALD films were 8.2 at. % in the plasma ABC 3 s and 6.2 at. % in the plasma AB 6 s films, whereas PEALD films from $AlMe_3$ and NH_3 plasma have been reported to have H concentrations of 14–27 at. %.[11,15,18]

IV. SUMMARY AND CONCLUSIONS

Crystalline AlN films with preferential (002) orientation were deposited from $AlCl_3$ on an amorphous starting surface with low impurity levels. The thermal AlN film had a low degree of crystallinity at 475 °C as observed from the XRD and TEM and residual chlorine concentration of 3.8 at. %. Based on zone models of thin film growth, higher temperatures, e.g., >500 °C, are suggested to improve crystallinity. Higher temperature would also result in lower Cl residues because of higher NH_3 reactivity. However, these temperatures are above the typical process temperature limit for ALD systems. Our PEALD AlN films had a higher degree of crystallinity and a lower impurity concentration with as low as 0.1 at. % of Cl. In addition, the PEALD allowed film stress control and AlN films with tensile, compressive, and close to zero stress were deposited. Hence, the PEALD is the suggested route toward high quality AlN films from $AlCl_3$.

The results from PEALD AlN encourage further experiments, such as the use of a growth promoting seed layer, to improve crystal quality for possible piezoelectric applications. ALD offers unmatched film thickness control for deposition of ultrathin AlN films, which might be a key in future NEMS applications. The required plasma-enhancement, however, impairs film conformality compared to thermal AlN, but low deposition temperatures combined with control over film properties could generate applications in which either MOCVD or sputtering is not possible or is inadequate.

ACKNOWLEDGMENTS

The OtaNano research infrastructure is acknowledged for providing facilities for research. This research was supported by the Finnish Cultural Foundation, ECSEL Joint Undertaking project InForMed, Grant No. 2014-2-662155 and the Academy of Finland Center of Excellence in Nuclear and Accelerator Based Physics (Ref. 251353). R. L. Puurunen is thanked for fruitful discussions. Andreas Graff (Fraunhofer IMWS CAM) is thanked for some of the TEM work.

[1]P. Ivaldi, J. Abergel, M. H. Matheny, L. G. Villanueva, R. B. Karabalin, M. L. Roukes, P. Andreucci, S. Hentz, and E. Defaÿ, J. Micromech. Microeng. **21**, 085023 (2011).
[2]U. Zaghloul and G. Piazza, Appl. Phys. Lett. **104**, 253101 (2014).
[3]J. R. Shealy, V. Kaper, V. Tilak, J. A. Smart, B. Green, and L. F. Eastman, J. Phys.: Condens. Matter. **14**, 3499 (2002).
[4]M. Kanamura, T. Ohki, T. Kikkawa, K. Imanishi, T. Imada, A. Yamada, and N. Hara, IEEE Electron Device Lett. **31**, 189 (2010).
[5]Y. Taniyasu, M. Kasu, and T. Makimoto, Nature **441**, 325 (2006).
[6]M. Kneissl *et al*., Semicond. Sci. Technol. **26**, 014036 (2011).
[7]E. Iborra, J. Olivares, M. Clement, L. Vergara, A. Sanz-Hervás, and J. Sangrador, Sens. Actuators, A **115**, 501 (2004).
[8]K. Tonisch, V. Cimalla, Ch. Foerster, H. Romanus, O. Ambacher, and D. Dontsov, Sens. Actuators, A **132**, 658 (2006).
[9]D. Riihelä, M. Ritala, R. Matero, M. Leskelä, J. Jokinen, and P. Haussalo, Chem. Vap. Deposition **2**, 277 (1996).
[10]H. van Bui, M. D. Nguyen, F. B. Wiggers, A. A. I. Aarnink, M. P. de Jong, and A. Y. Kovalgin, ECS J. Solid State Sci. Technol. **3**, P101 (2014).
[11]M. Bosund, T. Sajavaara, M. Laitinen, T. Huhtio, M. Putkonen, V.-M. Airaksinen, and H. Lipsanen, Appl. Surf. Sci. **257**, 7827 (2011).
[12]C. Ozgit, I. Donmez, M. Alevli, and N. Biyikli, Thin Solid Films **520**, 2750 (2012).
[13]M. Alevli, C. Ozgit, I. Donmez, and N. Biykli, Phys. Status Solidi A **209**, 266 (2012).
[14]N. Nepal, S. B. Qadri, J. K. Hite, N. A. Mahadik, M. A. Mastro, and C. R. Eddy, Jr., Appl. Phys. Lett. **103**, 082110 (2013).
[15]A. P. Perros, H. Hakola, T. Sajavaara, T. Huhtio, and H. Lipsanen, J. Phys. D: Appl. Phys. **46**, 505502 (2013).
[16]S. Goerke *et al*., Appl. Surf. Sci. **338**, 35 (2015).
[17]H. Van Bui, F. B. Wiggers, A. Gupta, M. D. Nguyen, A. A. I. Aarnink, M. P. de Jong, and A. Y. Kovalgin, J. Vac. Sci. Technol., A **33**, 01A111 (2015).
[18]M. Broas, P. Sippola, T. Sajavaara, V. Vuorinen, A. P. Perros, H. Lipsanen, and M. Paulasto-Kröckel, J. Vac. Sci. Technol., A **34**, 041506 (2016).
[19]V. A. Tarala, A. S. Altakhov, M. G. Ambartsumov, and V. Ya. Martens, Tech. Phys. Lett. **43**, 74 (2017).
[20]V. Miikkulainen, M. Leskelä, M. Ritala, and R. L. Puurunen, J. Appl. Phys. **113**, 021301 (2013).
[21]R. L. Puurunen, M. Lindblad, A. Root, and A. O. I. Krause, Phys. Chem. Chem. Phys. **3**, 1093 (2001).
[22]H. B. Profijt, S. E. Potts, M. C. M. van de Sanden, and W. M. M. Kessels, J. Vac. Sci. Technol., A **29**, 050801 (2011).
[23]M. Broas, H. Jiang, A. Graff, T. Sajavaara, V. Vuorinen, and M. Paulasto-Kröckel, Appl. Phys. Lett. **111**, 141606 (2017).
[24]K.-E. Elers, M. Ritala, M. Leskelä, and L.-S. Johansson, J. Phys. IV France **5**, C5-1021 (1995).
[25]J. Jokinen, P. Haussalo, J. Keinonen, M. Ritala, D. Riihelä, and M. Leskelä, Thin Solid Films **289**, 159 (1996).
[26]Y. J. Lee and S.-W. Kang, Thin Solid Films **446**, 227 (2004).
[27]Y. J. Lee, J. Cryst. Growth **266**, 568 (2004).
[28]H. B. Profijt, M. C. M. van de Sanden, and W. M. M. Kessels, J. Vac. Sci. Technol., A **31**, 01A106 (2013).
[29]O. M. E. Ylivaara *et al*., Thin Solid Films **552**, 124 (2014).
[30]J. Tiilikainen, J. M. Tilli, V. Bosund, M. Mattila, T. Hakkarainen, V. M. Airaksinen, and H. Lipsanen, J. Phys. D: Appl. Phys. **40**, 215 (2007).
[31]M. Laitinen, M. Rossi, J. Julin, and T. Sajavaara, Nucl. Instrum. Methods, B **337**, 55 (2014).
[32]K. Arstila *et al*., Nucl. Instrum. Methods., B **331**, 34 (2014).
[33]H. Schulz and K. H. Thiemann, Solid State Commun. **23**, 815 (1977).
[34]"Inorganic crystal structure database," https://icsd.fiz-karlsruhe.de/.
[35]G. F. Iriarte, J. G. Rodríguez, and F. Calle, Mater. Res. Bull. **45**, 1039 (2010).